Available online at www.sciencedirect.com
SCIENCE DIRECT®
Engineering Structures 27 (2005) 662–674
ENGINEERING STRUCTURES
www.elsevier.com/locate/engstruct

Design of tuned mass dampers incorporating wire rope springs: Part II: Simple design method

Rafik R. Gerges*, Barry J. Vickery

Alan G. Davenport Wind Engineering Group, Department of Civil and Environmental Engineering, Faculty of Engineering Science, The University of Western Ontario, London, Ontario, Canada N6A 5B9

Received 17 November 2003; received in revised form 26 November 2004; accepted 3 December 2004
Available online 5 March 2005

Abstract

A weighted-average technique to calculate the response of a structure equipped with a wire rope spring tuned mass damper, TMD, is presented. The probability distribution of structure-TMD relative displacement envelope is assumed to be of the Rayleigh-type and is used as a weighting function in averaging the amplitude-dependent response. The method is verified by comparing the calculated response with the measurements obtained from the experiments. Further, design charts are developed for structures subject to a white noise random force. The charts are in the form of contour plots for the equivalent viscous damping ratio, provided by the TMD, and the ratio of root-mean-square (RMS) relative displacement to RMS primary system displacement. The use of the design charts is demonstrated by a design example.

Keywords: Averaging; Design; Earthquake; Non-linear; Passive control; Probability; Tuned mass damper; Wind; Wire rope

1. Introduction

A general dynamic characterisation of wire rope springs was achieved in terms of amplitude-dependent effective stiffness and equivalent viscous damping as discussed in part I. When the amplitude-dependent stiffness and damping are substituted into the equations of motion of a two-degree of freedom system, TDOF, representing a structure equipped with a tuned mass damper (TMD) as shown in Fig. 1, the resulting response is dependent on the relative displacement amplitude.

Natural loads such as wind and earthquakes are excitations that cover a range of amplitudes and frequencies and hence the TDOF system response also contains a range of amplitudes. If the probability distribution of the structure-TMD relative displacement envelope is defined, it can be used as a weighting function in averaging the amplitude-dependent response. Through an iterative process the response of the non-linear TDOF system can be predicted, using the frequency-domain analysis, for a given excitation spectrum. To verify the prediction method, calculated responses are compared with experimental results described elsewhere [1,2].

Design charts for pendulum-type TMD's are developed. The random force applied to the primary structure is assumed to have a white noise spectrum. A contour plot for the equivalent viscous damping ratio, provided by the TMD, is presented and can be used to predict the primary system response. Additionally, a contour plot for the ratio of root-mean-square, RMS, relative displacement to RMS primary system displacement is provided, which allows the relative structure-TMD displacement to be predicted. Both the equivalent viscous damping ratio and the RMS displacement ratio are functions of the mass ratio, of auxiliary to primary system, and the normalised RMS relative displacement. The use of the design charts is demonstrated by an example.

* Corresponding address: Nabih Youssef & Associates Structural Engineers, 800 Wilshire Boulevard, Suite 510, Los Angeles, CA, USA. Tel.: +1 213 362 0707; fax: +1 213 688 3018.
E-mail addresses: rgerges@nyase.com, rafik_gerges@yahoo.ca (R.R. Gerges).

0141-0296/$ - see front matter © 2005 Elsevier Ltd. All rights reserved.
doi:10.1016/j.engstruct.2004.12.014

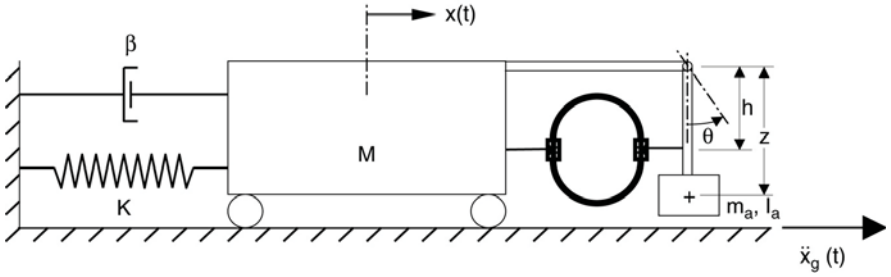

Fig. 1. Single-degree of freedom system equipped with wire rope spring pendulum-type TMD and subjected to base acceleration.

2. Response predictions

2.1. Frequency response functions

Expressions for the complex frequency response functions H_x and H_θ were derived by Gerges [1] and are given in Appendix A. x is the primary system displacement and θ is the auxiliary system rotation (see Fig. 1). Both H_x and H_θ are dimensionless and are described in terms of the non-dimensional parameters r_a, f_r, β, β_a, μ and g. μ is the mass ratio ($\mu = m_a/M$) and $r_a = I_a/m_a z^2$; I_a is the mass moment of inertia of the auxiliary system about the pivot, m_a is the auxiliary mass and z is the distance between the pivot and the auxiliary system centre of mass (see Fig. 1). f_r is the frequency ratio between the auxiliary system and the primary system (ω_a/ω_n), β is the damping ratio of the primary system, β_a is the damping ratio of the auxiliary system and g is the frequency normalised by the natural frequency of the primary system (ω/ω_n). Both f_r and β_a are dependent on the relative displacement amplitude, X_r, and consequently H_x and H_θ are dependent on X_r.

2.2. Probability distributions of excitation and response

Typical, experimentally obtained, probability distributions for the base acceleration excitation, $\ddot{x}_g$, the primary system displacement, x, and the auxiliary system rotation, θ, are shown in Fig. 2. Both the excitation $\ddot{x}_g$ and the response x have Gaussian probability distributions. This indicates that the structure maintains a near linear response despite the attachment of a non-linear TMD. θ has a peaked probability compared to the Gaussian distribution. The larger the response, the less peaked the distribution becomes, which is due to a less pronounced effect of the stick–slip behaviour. For design purposes, only large amplitudes are of importance, which may be approximated by a Gaussian distribution. For a narrow-band Gaussian process with zero mean, Crandell and Mark [3] showed that the probability density function, PDF, of the envelope follows the well known Rayleigh distribution.

2.3. Averaging technique

The response of a linear TDOF system subjected to a random base acceleration, $\ddot{x}_g$, can be obtained, for small θ, based on the random vibration theory as

$$\tilde{x}^2 = \frac{1}{\omega_n^3} \int_0^\infty S_{\ddot{x}_g}(g) |H_x(\mathrm{i}g)|^2 \, \mathrm{d}g \tag{1}$$

and

$$\tilde{x}_r^2 = \left(\frac{h}{z}\right)^2 \frac{1}{\omega_n^3} \int_0^\infty S_{\ddot{x}_g}(g) |H_\theta(\mathrm{i}g)|^2 \, \mathrm{d}g \tag{2}$$

where $\tilde{x}$ and $\tilde{x}_r$ are the RMS primary system displacement and the RMS relative displacement at the spring attachment location, respectively, for an excitation with a zero mean. $S_{\ddot{x}_g}(g)$ is the spectral density of the base acceleration and h is the distance between the pivot and the spring attachment point (see Fig. 1).

For a linear structure equipped with a wire rope spring TMD, both H_x and H_θ are amplitude-dependent. Since X_r was assumed to take the Rayleigh distribution form, its PDF, $p(X_r, \tilde{x}_r)$, is used as a weighting function to average the response over a range of amplitudes as follows

$$\tilde{x}^2 = \frac{1}{\omega_n^3} \int_0^{x_r^L} \int_0^\infty S_{\ddot{x}_g}(g) |H_x(\mathrm{i}g, X_r)|^2 \times p(X_r, \tilde{x}_r) \, \mathrm{d}g \, \mathrm{d}X_r \tag{3}$$

and

$$\tilde{x}_r^2 = \left(\frac{h}{z}\right)^2 \frac{1}{\omega_n^3} \int_0^{x_r^L} \int_0^\infty S_{\ddot{x}_g}(g) |H_\theta(\mathrm{i}g, X_r)|^2 \times p(X_r, x_r) \, \mathrm{d}g \, \mathrm{d}X_r \tag{4}$$

where x_r^L is the limiting relative displacement.

3. Comparison with experimental results

3.1. Frequency response functions

If $S_{\ddot{x}_g}(g)$ is considered to be constant in Eqs. (3) and (4) and since the double integral is interchangeable, averaged frequency response functions are obtained as

$$\overline{|H_x(\mathrm{i}g, \tilde{x}_r)|} = \sqrt{\int_0^{x_r^L} |H_x(\mathrm{i}g, X_r)|^2 p(X_r, \tilde{x}_r) \, \mathrm{d}X_r} \tag{5}$$

and

$$\overline{|H_\theta(\mathrm{i}g, \tilde{x}_r)|} = \sqrt{\int_0^{x_r^L} |H_\theta(\mathrm{i}g, X_r)|^2 p(X_r, \tilde{x}_r) \, \mathrm{d}X_r} \tag{6}$$

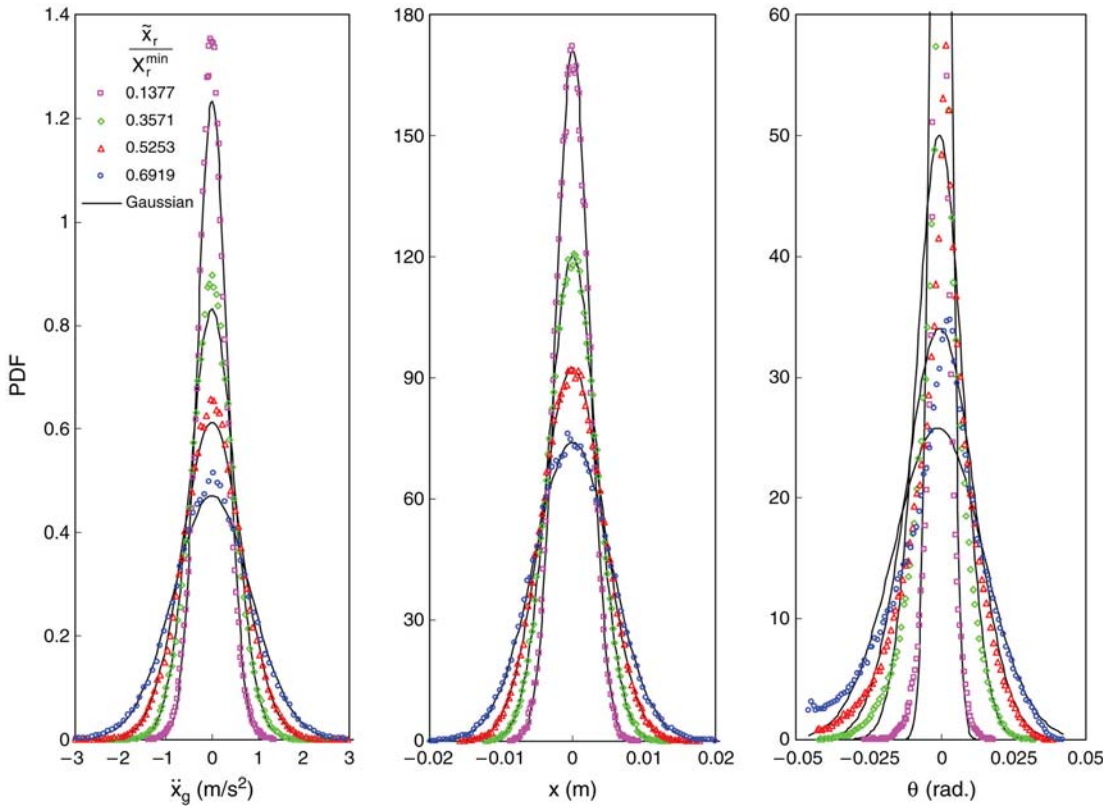

Fig. 2. Typical probability distributions for base acceleration, primary system displacement and auxiliary system rotation.

for the primary system displacement and the auxiliary system rotation, respectively.

The averaged frequency response functions are comparable to the experimentally obtained ones for the same $\tilde{x}_r$ value. Fig. 3 shows 3-D plots for the frequency response functions for two different mass ratios and employing "spring #1", the dimensions and properties of which are given in part I. Each of the 3-D plots describes the frequency response as a function of both the normalised RMS relative displacement, $\tilde{x}_r/X_r^{\min}$, and the forcing ratio, g. $X_r^{\min}$ is the relative displacement amplitude corresponding to minimum effective stiffness, $k^{\min}$, of a particular wire rope spring as discussed in part I. An interesting feature that can be observed is the lesser dependence of the frequency response functions on the relative displacement beyond $\tilde{x}_r/X_r^{\min} \approx 0.4$. This observation is of great importance to designers since uncertainties exist in estimating the excitation level. It also agrees with the findings of the parametric experimental study [1,2].

Experimentally obtained frequency response functions are plotted in Fig. 3 together with line plots, following the predicted surface, at the specific $\tilde{x}_r/X_r^{\min}$ values. In general, the predicted values are in a good agreement with the experiments. For $\mu = 0.116$, conservative predictions are observed for the largest two $\tilde{x}_r/X_r^{\min}$ values (see Fig. 3(a), (b)) and are attributed to the extra energy dissipated by the visco-elastic stop while impact was assumed to be perfectly elastic in the prediction process. For $\mu = 0.0345$, a good agreement for $|\overline{H_x(ig, \tilde{x}_r)}|$ values is seen while conservative predictions are obtained for $|\overline{H_\theta(ig, \tilde{x}_r)}|$ (see Fig. 3(c), (d)).

3.2. RMS response

Since $\tilde{x}_r$ appears on both sides of Eq. (4), iterations are required to evaluate $\tilde{x}_r$ and then it can be directly substituted into Eq. (3) to evaluate $\tilde{x}$. The double integral was evaluated numerically using the trapezoidal rule. Ratios of predicted to measured $\tilde{x}$ and $\tilde{x}_r$ are shown in Table 1. Among the sixty-four cases listed, there are only two cases where $\tilde{x}$ was underestimated and for all the others predictions were conservative. For $\tilde{x}_r$ ratios, reasonable fluctuations about unity are observed.

For a general evaluation of the proposed prediction method, statistics of predicted to measured response ratios are given in Table 2. Four categories were considered as a combination of "Heavy" for $\mu \simeq 0.116$, "Light" for $\mu \simeq 0.035$, "Single" for single wire rope spring on one side of the pendulum and "Double" for two springs on both sides of the pendulum [1,2]. For a 95% confidence level and considering all experimental results, ratios for $\tilde{x}$ lie between 1.224 and 0.968 and range from 1.237 to 0.761 for $\tilde{x}_r$ ratios. Fig. 4 shows the variation of $\tilde{x}$ and $\tilde{x}_r$ ratios versus $\tilde{x}_r/X_r^{\min}$. The overestimation of $\tilde{x}$ is increasing as $\tilde{x}_r/X_r^{\min}$ increases since

Table 1
Comparison between predicted and measured response under different arrangements and excitations

Experimental parameters								Ratio of predicted to measured							
μ ratio	r_a ratio	z mm	h mm	$\frac{k^{opt}}{k^{min}}$	$\frac{x_r^L}{X_r^{min}}$	Impact	$\frac{\tilde{x}_r}{X_r^{min}}$	$\tilde{x}$	$\tilde{x}_r$	PF_x (1 h)	PF_x (6 min)	PF_r (1 h)	PF_r (6 min)	PF_r [a] (1 h)	PF_r [a] (6 min)
(a) Spring # 1															
0.116	1.095	1154	994.8	1.046	1.877	No	0.1377	1.060	1.049	1.113	1.036	0.517	0.531	0.951	0.977
					1.901	No	0.3571	1.181	0.986	1.084	1.015	0.822	0.759	0.958	0.884
					1.931	Yes	0.5253	1.170	1.008	1.074	1.016	0.984	0.989	–	–
					2.000	Yes	0.6919	1.205	1.045	1.074	0.976	0.911	0.914	–	–
0.116	1.097	1150	930.3	1.185	1.657	No	0.1524	1.098	0.949	1.077	1.004	0.538	0.566	0.954	1.003
					1.657	No	0.3175	1.148	0.977	1.056	0.986	0.835	0.757	1.031	0.935
					1.662	Yes	0.4944	1.202	1.018	1.057	1.007	0.948	0.950	–	–
0.116	1.099	1146	866.8	1.360	1.657	No	0.1700	1.118	0.896	1.051	0.985	0.609	0.641	1.033	1.088
					1.670	No	0.3120	1.127	0.934	1.042	0.976	0.815	0.755	1.016	0.941
					1.668	Yes	0.4829	1.207	0.986	1.033	1.003	0.994	0.996	–	–
					1.706	Yes	0.4863	1.206	0.983	1.041	1.002	0.981	0.983	–	–
0.0345	1.479	582	333.4	1.150	1.566	No	0.0988	1.026	1.064	1.057	0.991	0.501	0.470	1.018	0.955
					1.609	No	0.1892	1.050	0.970	1.056	0.984	0.601	0.563	0.973	0.911
					1.610	No	0.3221	1.077	0.917	1.039	0.963	1.019	0.922	1.249	1.130
0.0345	1.500	576	304.8	1.365	1.567	No	0.1017	1.029	1.029	1.059	0.987	0.512	0.510	1.033	1.029
					1.567	No	0.1926	1.060	0.952	1.060	0.982	0.570	0.567	0.915	0.910
					1.599	No	0.3020	1.088	0.934	1.053	0.976	0.820	0.727	1.040	0.922
0.0345	1.519	570	279.4	1.615	1.567	No	0.1093	1.039	0.984	1.057	0.991	0.543	0.552	1.074	1.092
					1.567	No	0.2020	1.062	0.867	1.055	0.982	0.627	0.619	0.984	0.972
					1.610	No	0.3040	1.072	0.838	1.043	0.974	0.817	0.741	1.033	0.937
(b) Springs # 2a and 2b															
0.117	1.084	1162	993.8	0.945	1.753	No	0.119	1.043	1.075	1.098	1.037	0.529	0.574	1.021	1.108
					1.753	No	0.281	1.125	1.082	1.125	1.027	0.795	0.746	1.049	0.985
					1.923	No	0.497	1.166	1.033	1.133	1.020	0.974	1.013	–	–
					2.301	Yes	0.700	1.194	1.039	1.109	0.991	1.008	1.078	–	–
0.117	1.087	1157	930.3	1.071	1.753	No	0.156	1.138	0.910	1.094	1.025	0.608	0.637	1.068	1.119
					1.753	No	0.317	1.177	0.972	1.085	1.006	0.884	0.838	1.093	1.036
(c) Spring #3															
0.116	1.080	1169	993.8	1.020	1.497	No	0.143	1.011	1.165	1.109	1.045	0.443	0.472	0.804	0.857
					1.571	No	0.266	1.078	1.114	1.118	1.027	0.739	0.659	1.005	0.896
					1.530	Yes	0.415	1.126	1.078	1.086	1.019	0.924	0.927	–	–
					1.575	Yes	0.475	1.142	1.071	1.043	0.989	0.907	0.912	–	–
0.116	1.140	1164	930.3	1.130	1.497	No	0.072	1.015	1.072	1.107	1.039	0.445	0.468	0.969	1.020
					1.497	No	0.170	1.095	0.938	1.097	1.020	0.502	0.512	0.852	0.869
					1.600	Yes	0.300	1.153	0.943	1.076	0.999	0.818	0.720	1.042	0.917
					1.603	Yes	0.445	1.211	0.970	1.114	1.034	1.201	1.011	–	–
0.116	1.084	1159	866.8	1.324	1.572	No	0.081	1.035	1.014	1.099	1.034	0.461	0.478	0.981	1.017
					1.572	No	0.188	1.115	0.891	1.084	1.005	0.554	0.569	0.899	0.924
					1.608	Yes	0.314	1.137	0.898	1.062	0.990	0.847	0.747	1.052	0.928
					1.628	Yes	0.451	1.178	0.932	1.100	1.022	1.041	1.048	–	–
0.0341	1.417	601	333.4	1.123	1.572	No	0.092	1.032	1.072	1.065	0.990	0.462	0.423	0.956	0.875
					1.572	No	0.083	1.028	1.184	1.063	0.989	0.457	0.421	0.968	0.891
0.0341	1.440	594	304.8	1.330	1.572	No	0.148	1.046	0.881	1.042	0.966	0.677	0.618	1.214	1.108
0.0341	1.461	587	279.4	1.573	1.572	No	0.104	1.051	0.906	1.062	0.987	0.502	0.508	1.007	1.019
					1.572	No	0.150	1.059	0.777	0.956	0.966	0.473	0.539	0.844	0.961
					1.572	No	0.159	1.061	0.840	1.046	0.971	0.520	0.529	0.907	0.922
(d) Springs # 4a and 4b															
0.117	1.084	1162	993.8	0.999	1.467	No	0.055	0.978	1.296	1.078	1.036	0.348	0.438	0.792	0.997
					1.467	No	0.109	0.987	1.303	1.086	1.036	0.439	0.473	0.869	0.937

(*continued on next page*)

Table 1 (*continued*)

Experimental parameters								Ratio of predicted to measured							
μ ratio	r_a ratio	z mm	h mm	$\frac{k^{opt}}{k^{min}}$	$\frac{x_r^L}{X_r^{min}}$	Impact	$\frac{\tilde{x}_r}{X_r^{min}}$	$\tilde{x}$	$\tilde{x}_r$	PF_x (1 h)	PF_x (6 min)	PF_r (1 h)	PF_r (6 min)	PF_r[a] (1 h)	PF_r[a] (6 min)
					1.467	No	0.216	1.049	1.247	1.107	1.028	0.657	0.619	0.998	0.940
					1.776	Yes	0.371	1.122	1.143	1.106	1.020	0.883	0.875	–	–
0.117	1.087	1157	930.3	1.130	1.467	No	0.073	1.008	1.086	1.107	1.043	0.462	0.506	1.004	1.100
					1.467	No	0.148	1.057	1.028	1.106	1.029	0.557	0.568	0.998	1.018
					1.557	No	0.265	1.120	1.049	1.110	1.024	0.752	0.715	1.025	0.975
					1.803	Yes	0.406	1.174	1.040	1.102	1.017	0.974	0.945	–	–
0.117	1.089	1152	866.8	1.297	1.540	No	0.094	1.096	0.854	1.086	1.020	0.537	0.568	1.105	1.169
					1.540	No	0.178	1.125	0.880	1.090	1.012	0.664	0.670	1.105	1.115
					1.605	No	0.292	1.158	0.924	1.096	1.014	0.805	0.784	1.040	1.013
					1.784	No	0.418	1.192	0.950	1.085	1.009	1.054	0.966	1.162	1.065
					1.972	Yes	0.426	1.183	0.933	1.085	1.007	0.975	0.958	1.071	1.052
0.0354	1.442	586	333.4	1.101	1.540	No	0.087	1.033	1.101	1.039	0.982	0.462	0.446	0.968	0.935
					1.540	No	0.117	1.035	0.986	1.032	0.965	0.560	0.512	1.086	0.993
0.0354	1.466	578	304.8	1.305	1.513	No	0.043	1.025	1.351	1.058	0.994	0.430	0.412	1.010	0.967
					1.513	No	0.086	1.036	1.030	1.054	0.987	0.519	0.499	1.091	1.048
					1.513	No	0.133	1.049	0.901	1.010	0.965	0.680	0.624	1.266	1.162
0.0354	1.489	572	279.4	1.540	1.513	No	0.091	1.047	0.997	1.062	0.985	0.555	0.540	1.151	1.120
					1.513	No	0.137	1.069	0.735	0.903	1.055	0.578	0.703	1.065	1.296
					1.513	No	0.150	1.059	0.850	1.048	0.977	0.635	0.620	1.133	1.106

Underlined values are governed by stop location.

[a] Corrected peak factors.

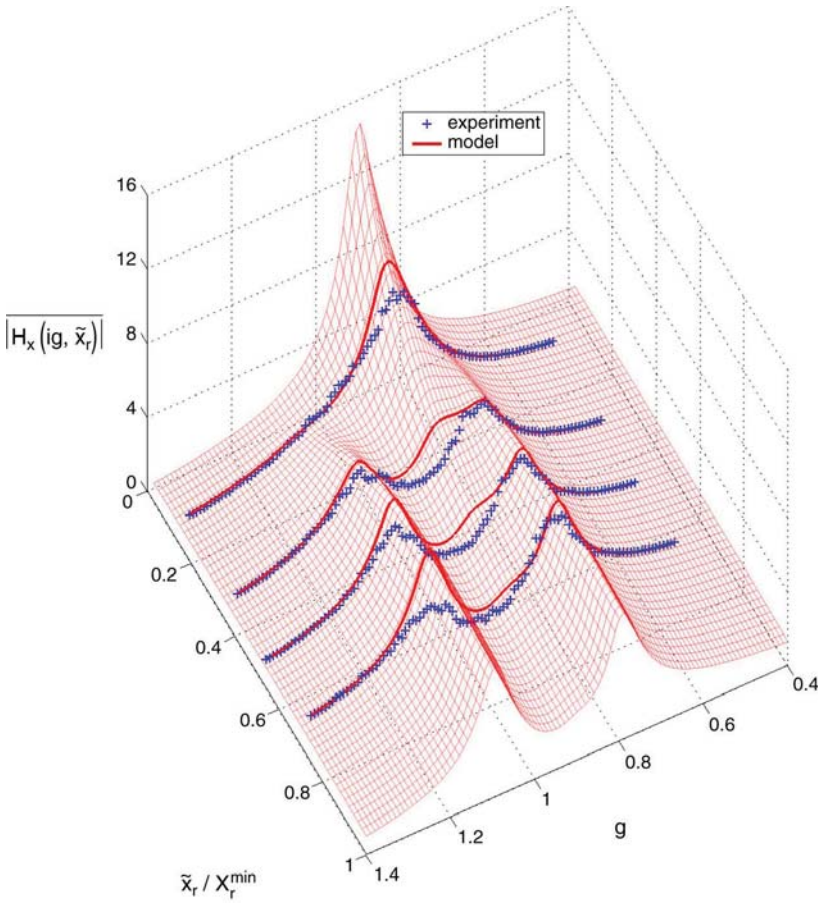

(a) Primary system displacement for mass ratio of 0.116 tuned at $1.046k^{min}$.

Fig. 3. 3-D plots of frequency response functions for spring # 1.

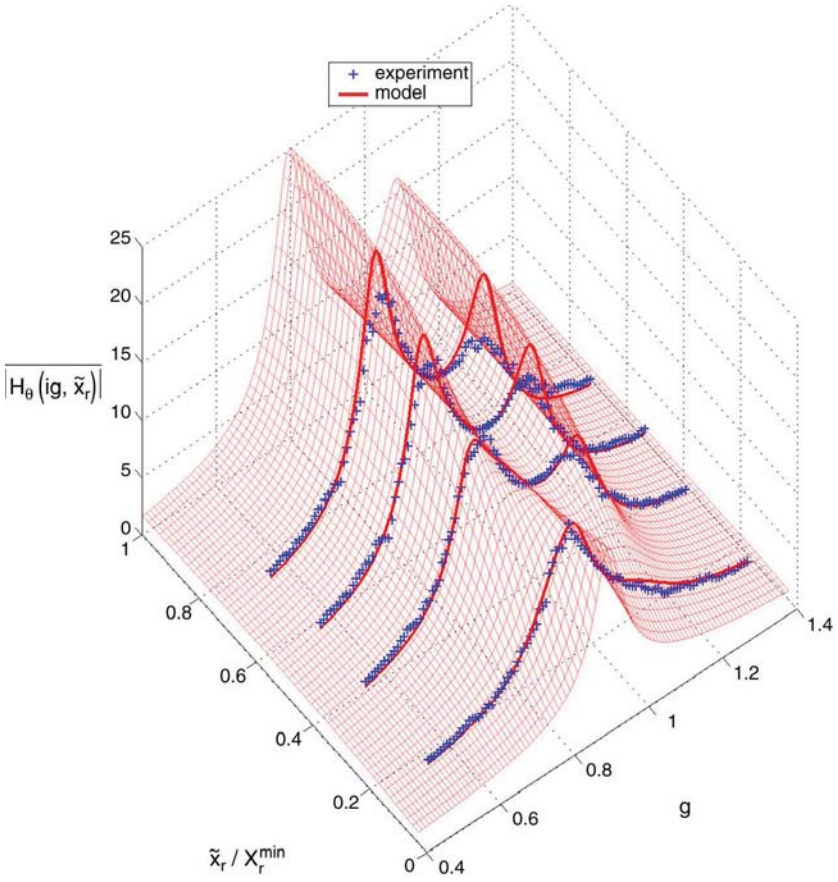

(b) Auxiliary system rotation for mass ratio of 0.116 tuned at $1.046k^{\min}$.

Fig. 3. (*continued*).

Table 2
Statistics of predicted to measured ratios

Data sets	$\tilde{x}$		$\tilde{x}_r$		PF_x (1 h)		PF_x (6 min)		PF_r[a] (1 h)		PF_r[a] (6 min)	
	mean	SD	mean	SD	mean	SD	mean	SD	mean	SD	mean	SD
Heavy-single	1.131	0.062	0.996	0.072	1.078	0.026	1.010	0.020	0.968	0.074	0.947	0.066
Heavy-double	1.110	0.070	1.044	0.131	1.099	0.014	1.021	0.013	1.027	0.093	1.042	0.070
Light-single	1.052	0.019	0.948	0.107	1.048	0.027	0.980	0.010	1.014	0.106	0.976	0.082
Light-double	1.044	0.015	0.994	0.184	1.026	0.052	0.989	0.029	1.096	0.091	1.078	0.118
All	1.096	0.064	0.999	0.119	1.071	0.037	1.004	0.024	1.018	0.098	1.003	0.093

[a] Corrected peak factors.

impact is more frequent and therefore the energy dissipated through the visco-elastic stop increases. The scatter of $\tilde{x}_r$ ratios decreases with the increase of $\tilde{x}_r / X_r^{\min}$ to about half in the range of 0.25 to 0.5 $\tilde{x}_r / X_r^{\min}$, which is the practical design range as explained in Section 3.3.

3.3. Peak factors

Peak values are of great importance for design of structures vulnerable to brittle failure. For a random dynamic response of a zero mean, the peak, $\hat{R}_d$, can be expressed as

$$\hat{R}_d = PF\ \tilde{R}_d \tag{7}$$

where PF is the peak factor and $\tilde{R}_d$ is the RMS dynamic response. An expression presented by Davenport [4,5] to calculate the peak factor for a Gaussian random process is in the form

$$PF = \sqrt{2\ \log_e(f_o T)} + \frac{0.5772}{\sqrt{2\log_e(f_o\ T)}} \tag{8}$$

where T is the duration of time over which the peak factor is calculated and f_o is the expected response frequency [3] and is given by

$$f_o = \frac{\omega_n}{2\pi}\sqrt{\frac{\int_0^\infty g^2 S_{R_d}(g)\,\mathrm{d}g}{\int_0^\infty S_{R_d}(g)\,\mathrm{d}g}} \tag{9}$$

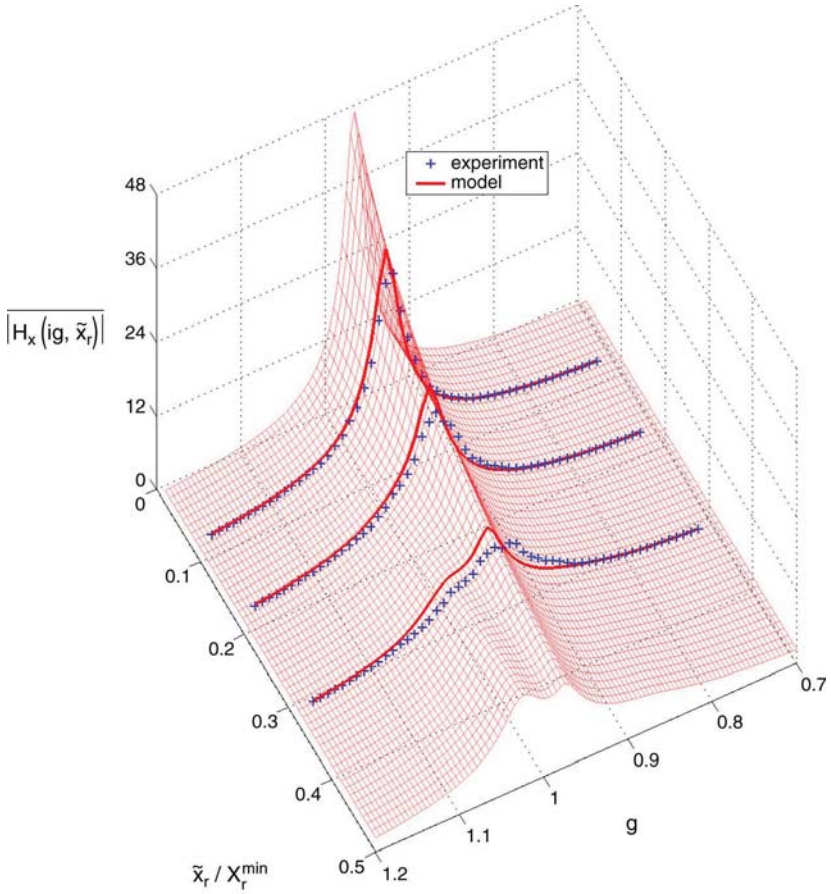

(c) Primary system displacement for mass ratio of 0.0345 tuned at $1.150k^{\min}$.

Fig. 3. (*continued*).

where $S_{R_d}(g)$ is the spectrum of a particular dynamic response.

The peak factor values for primary system displacement, PF_x, and auxiliary system relative displacement, PF_r, were evaluated numerically. Ratios of predicted to experimentally obtained peak factors, for one hour and six minute sampling times, are listed in Table 1. Predictions for PF_x are mostly conservative while PF_r values are considerably underestimated. The underestimation of PF_r is due to the stick–slip behaviour of the auxiliary system, which resulted in a peaked response more pronounced for small amplitudes. As the amplitude of the relative displacement increases, the PDF of auxiliary system response becomes less peaked approaching the Gaussian assumption and therefore predictions improve. For a very large relative displacement amplitude, PF_r predictions were governed by stop location and their values are underlined in Table 1.

To account for deviations from the Gaussian assumption, a correction factor is suggested. Ratios of measured to predicted PF_r are plotted versus $\tilde{x}_r/X_r^{\min}$ in Fig. 5. An expression for the correction factor is obtained, based on a least square fit, in the form

$$P_{CF} = 7.291\left(\frac{\tilde{x}_r}{X_r^{\min}}\right)^2 - 6.823\left(\frac{\tilde{x}_r}{X_r^{\min}}\right) + 2.622$$

$$\text{for} \quad \frac{\tilde{x}_r}{X_r^{\min}} < 0.47 \tag{10a}$$

$$P_{CF} = 1.09 \qquad \text{for } \frac{\tilde{x}_r}{X_r^{\min}} \geq 0.47. \tag{10b}$$

The corrected relative displacement peak factor is given by

$$PF_r^* = P_{CF}PF_r \tag{11}$$

for which, values are listed in Table 1.

Since the peak factor for Gaussian excited linear structures commonly ranges from 3.5 to 4.5 [5] and based on the expression for P_{CF}, provided by Eq. (10), estimations of normalised peak relative displacement, $\hat{x}_r/X_r^{\min}$, are shown in Fig. 6. For stop located at $1.5X_r^{\min}$, $\tilde{x}_r/X_r^{\min}$ design range is 0.22–0.37 depending on the natural frequency of the structure. This range can be increased to 0.40–0.53 for stop located at $2.0X_r^{\min}$. One can conclude that for most of the practical situations, $\tilde{x}_r/X_r^{\min}$ design values lie in between 0.22–0.53.

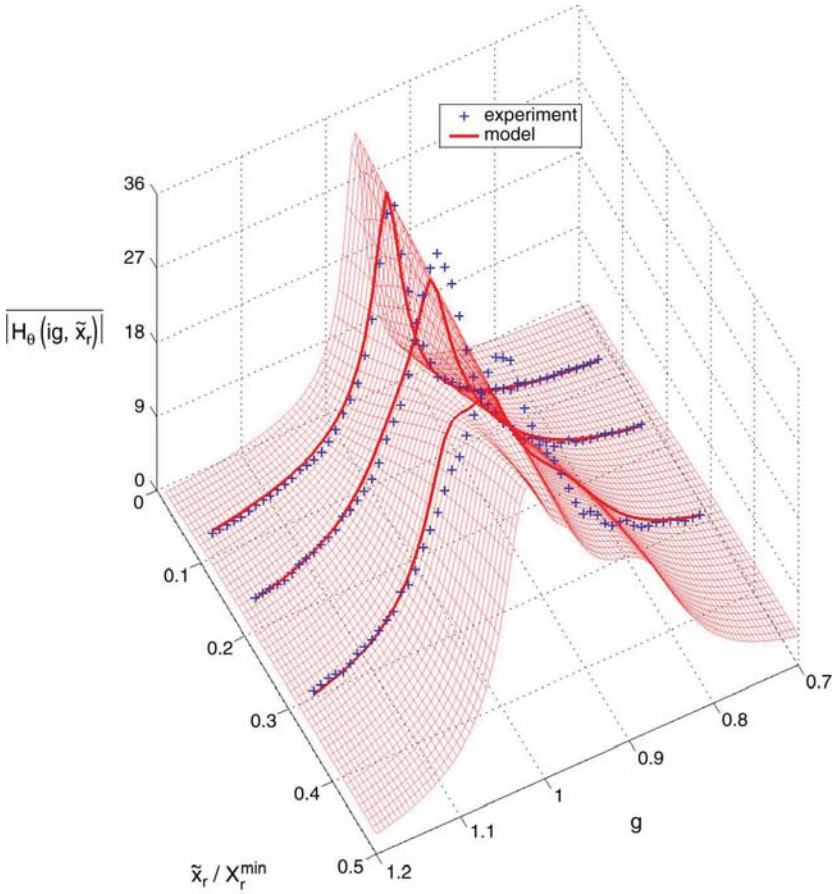

(d) Auxiliary system rotation for mass ratio of 0.0345 tuned at $1.150k^{\min}$.

Fig. 3. (*continued*).

Statistics of predicted to measured peak factor ratios are given in Table 2. Mean values in the near vicinity of unity are observed for both PF_x and PF_r^* including all categories. Little scatter is seen for PF_x and slightly larger scatter is seen in the case of PF_r^*. The variation of predicted to measured ratios with $\tilde{x}_r / X_r^{\min}$ is shown in Fig. 7. Fortunately, scatter in PF_r^* reduces with the increase of normalised $\tilde{x}_r$ values towards the design range.

4. Design method

4.1. TMD response parameters

Two non-dimensional parameters are fully representative of the linear TMD system as reported by Vickery and Davenport [6]. β_e and R are the equivalent viscous damping ratio provided by the TMD and the ratio of RMS displacement of primary system to auxiliary system, respectively. Closed form integral expressions for both β_e and R, for a structure excited by a white noise random force were derived in terms of H_x and H_θ [6]. Expressions for H_x and H_θ are given in Appendix A.

Following the proposed averaging technique, both mechanical admittance functions, of primary and auxiliary systems, are substituted by averaged ones. The average equivalent viscous damping ratio, $\bar{\beta}_e$, and the average RMS displacement ratio, $\bar{R}$, are given by

$$\bar{\beta}_e(\tilde{x}_r) = \frac{\pi}{4\int_0^\infty \overline{|H_x(ig, \tilde{x}_r)|}^2 \, dg} \tag{12}$$

and

$$\bar{R}(\tilde{x}_r) = \sqrt{\frac{\int_0^\infty \overline{|H_\theta(ig, x_r)|}^2 \, dg}{\int_0^\infty \overline{|H_x(ig, \tilde{x}_r)|}^2 \, dg}} \tag{13}$$

where $\overline{|H_x(ig, \tilde{x}_r)|}$ and $\overline{|H_\theta(ig, \tilde{x}_r)|}$ are given by Eqs. (5) and (6), respectively.

4.2. Design parameters

The stop location is usually chosen in the range of 1.5–2.0$X_r^{\min}$, depending on coil diameter to rope diameter ratio, and was conservatively taken as $1.5X_r^{\min}$ in this study. Mathematically, this was expressed by setting $x_r^L = 1.5X_r^{\min}$ in Eqs. (5) and (6). μ values ranging from 0.001 to 0.2 were

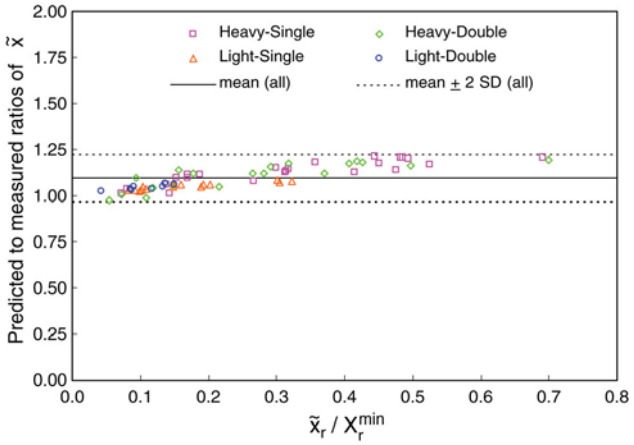

(a) Primary system displacement.

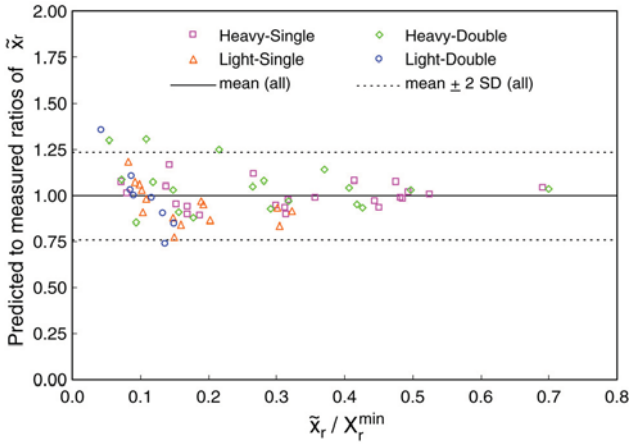

(b) Relative displacement.

Fig. 4. Predicted to measured RMS response ratios vs. normalised RMS relative displacement.

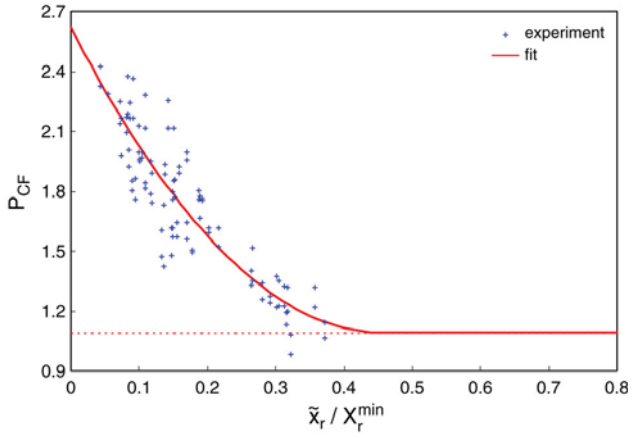

Fig. 5. Peak correction factor vs. normalised RMS relative displacement.

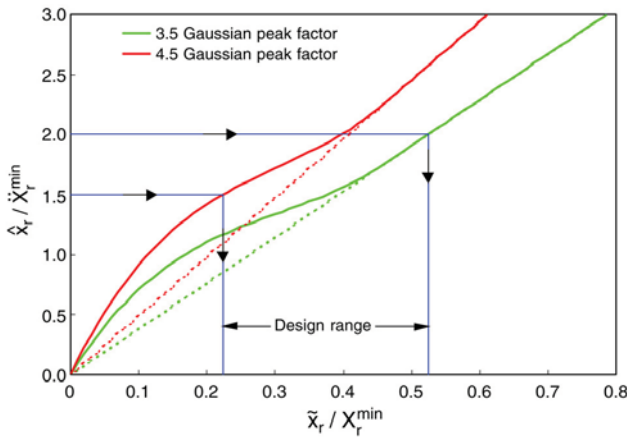

Fig. 6. Normalised peak relative displacement vs. normalised RMS relative displacement.

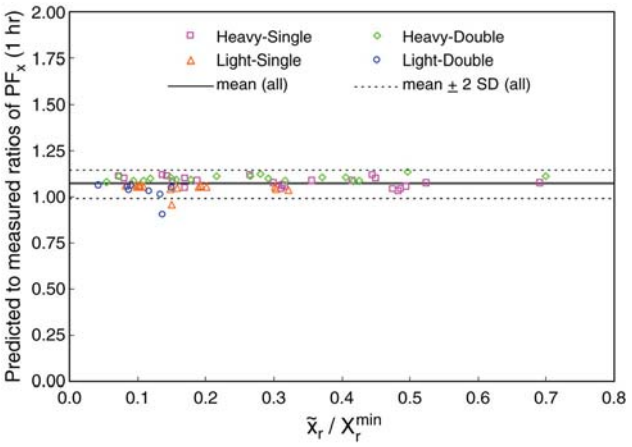

(a) Primary system displacement.

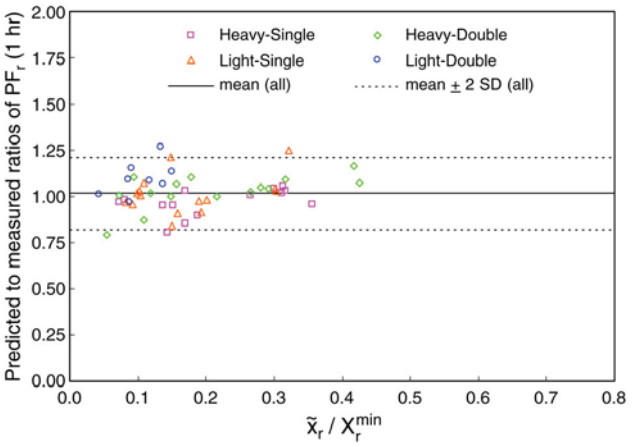

(b) Relative displacement.

Fig. 7. Predicted to measured peak factor ratios vs. normalised RMS relative displacement.

considered. r_a was chosen as 1.15 to allow for a reasonably stiff hanger.

The ratio of pendulum rotational stiffness, k_p^θ, to the minimum of that provided by wire rope spring, $k^{\min}h^2$, was chosen as 0.1. The increase of $k_p^\theta/k^{\min}h^2$ ratio enables the hanger length to be shortened. However, the small rotation assumption has to be maintained. From a performance point of view, increasing this ratio reduces the variation of the frequency ratio, f_r, about its optimum value, and therefore

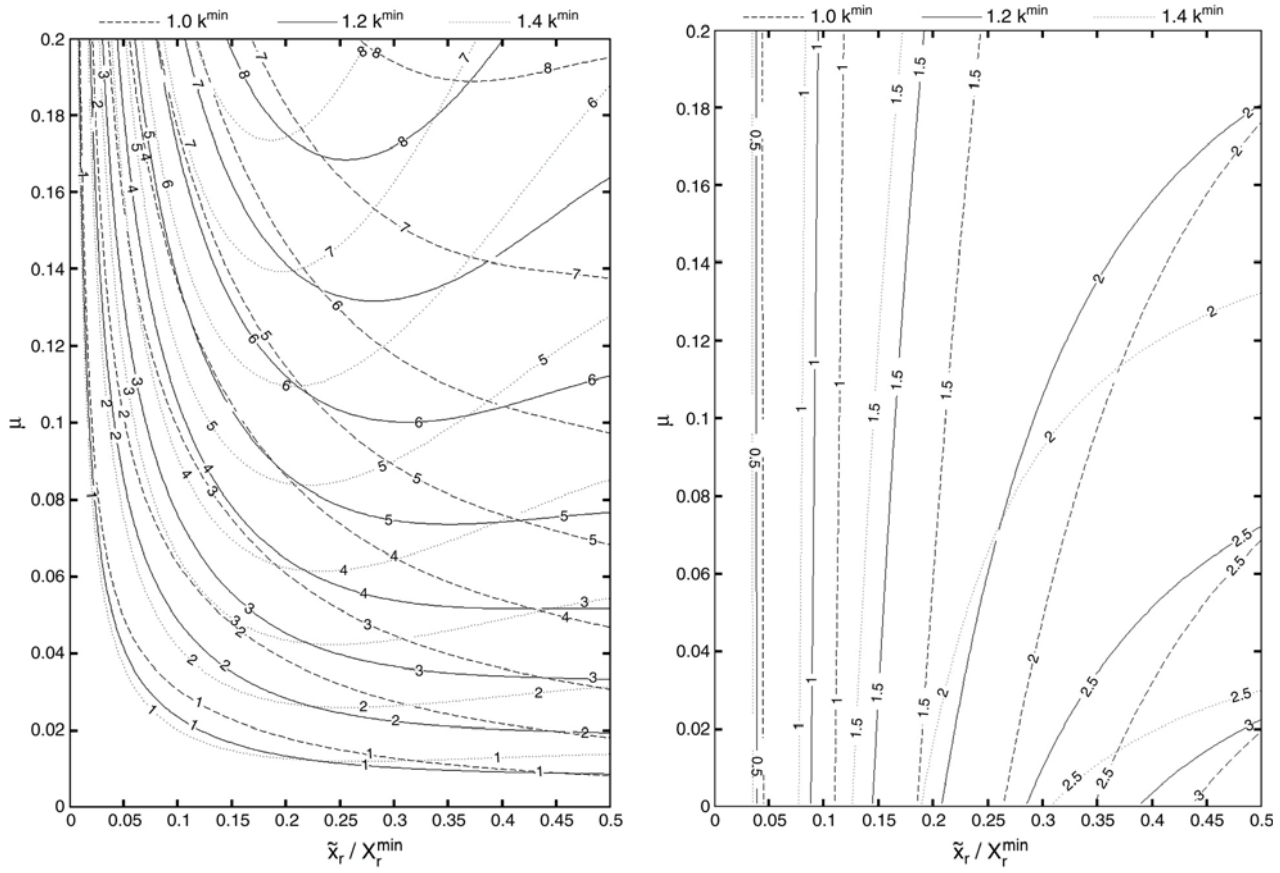

(a) Equivalent viscous damping ratio (% critical). (b) Root-mean-square response ratio.

Fig. 8. Contour plots for wire rope spring TMD response parameters.

increases the damping provided by the non-linear TMD. On the other hand, increasing $k_p^{\theta}/k^{\min}h^2$ ratio reduces the overall auxiliary system damping, β_a. Such a reduction in β_a shifts its value either away from or towards the optimum value depending on the μ and $\tilde{x}_r/X_r^{\min}$ values chosen for a particular design [1,2].

4.3. Design charts

Contour plots for the average equivalent viscous damping ratio provided by the TMD, $\bar{\beta}_e$, and the average RMS displacement ratio, $\bar{R}$ are shown in Fig. 8. Both $\bar{\beta}_e$ and $\bar{R}$ are described as functions of μ and $\tilde{x}_r/X_r^{\min}$.

The optimum value of f_r for a linear system, expressed as a function of μ, was derived [1] and is

$$f_r^{\text{opt}} = \frac{\sqrt{1+\left(1-\frac{1}{2r_a}\right)}}{1+\mu}. \tag{14}$$

The optimum tuning frequency for a TMD characterised by a displacement-dependent stiffness, is only possible at some chosen displacement amplitude(s). Three wire rope spring stiffness values, $k^{\min}$, $1.2k^{\min}$ and $1.4k^{\min}$, corresponding to different X_r values as discussed in part I, were chosen for optimum tuning. This variation in displacement amplitude, at which optimum frequency tuning is achieved, is considered to find the maximum $\bar{\beta}_e$ for a particular μ and $\tilde{x}_r/X_r^{\min}$ combination. It is also useful in determining the reduction in $\bar{\beta}_e$ due to frequency-off-tuning.

Fig. 8 (a) shows that $\bar{\beta}_e$ increases with the increase of μ, which is similar to a linear system. For a certain μ value, $\bar{\beta}_e$ increases with the increase of $\tilde{x}_r/X_r^{\min}$ up to its maximum value and then decreases. In other words, for each combination of μ and tuning stiffness, there is an optimum value for $\tilde{x}_r/X_r^{\min}$ at which $\bar{\beta}_e$ is maximised. Since designers get to choose a combination of μ and $\tilde{x}_r/X_r^{\min}$ values, the tuning stiffness should be varied to maximise $\bar{\beta}_e$ for this particular design. The maximum value of $\bar{\beta}_e$ corresponds to a larger $\tilde{x}_r/X_r^{\min}$ as the tuning stiffness decreases. This follows the same trend as the wire rope stiffness-amplitude relationship shown in part I. Also, contour lines become flatter as the tuning stiffness decreases since variations of f_r about its optimum value is less for a wider range of amplitudes.

The average RMS displacement ratio, $\bar{R}$, is shown in Fig. 8(b). It is almost independent of μ for small $\tilde{x}_r/X_r^{\min}$ values. As $\tilde{x}_r/X_r^{\min}$ increases, $\bar{R}$ shows slight dependence on μ and it becomes larger for smaller μ. For the largest $\tilde{x}_r/X_r^{\min}$ value considered, $\bar{R}$ value is comparable to that of

an optimum linear system, for large μ values. However, it is considerably smaller for small μ values.

Stick–slip behaviour was approximated by large stiffness and no damping of the auxiliary system for small $\tilde{x}_r/X_r^{\min}$ as discussed in part I and is well reflected in TMD response parameters. As $\tilde{x}_r/X_r^{\min}$ approaches zero both $\bar{\beta}_e$ and $\bar{R}$ also approach zero meaning that the auxiliary system sticks to the primary structure with no reduction in the mechanical admittance co-ordinate at the natural frequency.

5. Design example

5.1. Background

A sheeted framed tower with a height of 56 m and a square cross-section with a side length, D, of 2.3 m was observed to oscillate significantly in moderate winds. Table 3 shows the main dynamic properties of the tower. It is required to limit the maximum tip deflection to 200 mm to meet ultimate limit state design criteria.

Table 3
Tower dynamic properties

Total mass of the tower	60,480 kg
Vibration mode to be controlled	1st sway mode in both directions
Natural frequency of vibration mode	0.67 Hz
Modal mass of the stack at top	16,200 kg
Maximum permissible tip deflection	200 mm

5.2. Tower aerodynamics

Preliminary calculations showed that the drag deflection is about 20 mm. For an aspect ratio of 24, the Strouhal Number is about 0.13 and hence the critical wind speed for vortex shedding at 10 m height is about 35 km/h. Such a wind speed lies within the design range of the tower specific site. A conclusion was drawn that the severe motion is an across-wind response phenomenon.

For the across wind response, at the vortex shedding lock-in, a relationship between the RMS tip displacement, $\tilde{x}_{\text{tip}}$, and the inherent viscous damping ratio of the structure, β_{struct}, was developed, in a non-dimensional form based on Vickery and Steckley's work [7], as

$$\frac{\tilde{x}_{\text{tip}}}{D} = \frac{3.7 \times 10^{-3}}{\sqrt{\beta_{\text{struct}} - 0.010}} \tag{15}$$

and conservatively assumed a Gaussian peak factor, which is 4.1 for one hour wind event. To limit the peak tip displacement to 200 mm, an added damping ratio of 3.5% is required.

5.3. TMD design

A design point of $\tilde{x}_r/X_r^{\min} = 0.40$ is chosen for which the stop needs to be set at $1.8X_r^{\min}$ to achieve no impact. Considering uncertainties in the applied force, the required level of damping should be maintained for about ±20% of the $\tilde{x}_r/X_r^{\min}$ design value. An auxiliary system tuned at $1.2k^{\min}$ produces the largest $\bar{\beta}_e$, in the range of interest, and corresponds to a μ value of 0.044. For this μ value and $\tilde{x}_r/X_r^{\min}$ range, $\bar{R}$ ranges from 2.3 to 2.7.

Two pendulum-type TMD's are required, each for a principal direction of motion. The properties of the pendulum should be chosen to match the values for r_a and $k_p^\theta/k^{\min}h^2$ ratios upon which the design charts were based and to maintain small rotations. Wire rope spring dimensions and attachment point were chosen to accommodate the relative displacement with no stop impact, produce the required auxiliary system frequency, be reasonably distanced from the pivot to reduce secondary displacement, as discussed in part I, and, again, maintain $k_p^\theta/k^{\min}h^2$ ratios upon which the design charts were based. Properties of the pendulum and the wire rope spring are shown in Table 4.

Table 4
TMD design parameters

	Tuned	10% off tuned
Mass of the pendulum	713 kg	1102 kg
Distance between pendulum C. G. and pivot	3 m	3 m
Ratio of mass moment of inertia about pivot to that about C. G.	1.15	1.15
Distance between spring attachment point and pivot	1.25 m	1.24 m
Number of coils	10	12
Coil diameter	780 mm	720 mm
Wire rope diameter	38.1 mm	38.1 mm
Stop location	250 mm	230 mm

Another design that allows 10% error in the frequency ratio, f_r, is also presented. Such a design employs a larger μ value of 0.068. The 50% increase of the auxiliary system mass, in some situations, is more economical than on-site tuning, as required in the first design. To represent the off-tuned case, the design is carried on for $1.2k^{\min}$, however, the lowest $\bar{\beta}_e$ values for $1.0k^{\min}$ and $1.4k^{\min}$ were considered. On the other hand, the maximum $\bar{R}$ ratio of $1.0k^{\min}$, $1.2k^{\min}$ and $1.4k^{\min}$ was considered in the design.

6. Conclusions

An averaging technique is presented to predicted structure-TMD response in the frequency-domain. The technique employs the Rayleigh probability density function to weight the relative-displacement-dependent response. The predictions were found to be in a good agreement with experimentally obtained response statistics.

A correction for the relative displacement peak factor is presented in a form of a second order polynomial that depends on the normalised RMS relative displacement.

Table A.1(a)
Response parameters under base acceleration

$$H_X(\mathrm{ig}) = \frac{-g^2\,(-r_a+\mu-r_a\mu)+\mathrm{ig}(-2f_r r_a\beta_a-2f_r r_a\beta_a\mu)+(-f_r^2 r_a-f_r^2 r_a\mu)}{g^4(r_a-\mu+r_a\mu)-\mathrm{ig}^3(2r_a\beta+2f_r r_a\beta_a+2f_r r_a\beta_a\mu)-g^2(r_a+f_r^2 r_a+f_r^2 r_a\mu+4f_r r_a\beta\beta_a)+\mathrm{ig}(2f_r^2 r_a\beta+2f_r r_a\beta_a)+(f_r^2 r_a)}$$

$$H_\theta(\mathrm{ig}) = \frac{\mathrm{ig}(-2\beta)+(-1)}{g^4(r_a-\mu+r_a\mu)-\mathrm{ig}^3(2r_a\beta+2f_r r_a\beta_a+2f_r r_a\beta_a\mu)-g^2(r_a+f_r^2 r_a+f_r^2 r_a\mu+4f_r r_a\beta\beta_a)+\mathrm{ig}(2f_r^2 r_a\beta+2f_r r_a\beta_a)+(f_r^2 r_a)}$$

Table A.1(b)
Response parameters under dynamic force

$$H_X(\mathrm{ig}) = \frac{-g^2(r_a)+\mathrm{ig}(2f_r r_a\beta_a)+(f_r^2 r_a)}{g^4(r_a-\mu+r_a\mu)-\mathrm{ig}^3(2r_a\beta+2f_r r_a\beta_a+2f_r r_a\beta_a\mu)-g^2(r_a+f_r^2 r_a+f_r^2 r_a\mu+4f_r r_a\beta\beta_a)+\mathrm{ig}(2f_r^2 r_a\beta+2f_r r_a\beta_a)+(f_r^2 r_a)}$$

$$H_\theta(\mathrm{ig}) = \frac{-g^2(-1)}{g^4(r_a-\mu+r_a\mu)-\mathrm{ig}^3(2r_a\beta+2f_r r_a\beta_a+2f_r r_a\beta_a\mu)-g^2(r_a+f_r^2 r_a+f_r^2 r_a\mu+4f_r r_a\beta\beta_a)+\mathrm{ig}(2f_r^2 r_a\beta+2f_r r_a\beta_a)+(f_r^2 r_a)}$$

The peak factors for the primary system displacement were accurately predicted by the Gaussian peak factor expression. This showed that the linear response of the primary system is maintained despite the attachment of a non-linear tuned mass damper.

Design charts were developed for wire rope spring tuned mass dampers attached to a structure presentable by a single degree of freedom system and subject to white noise random force. Contour plots for the equivalent viscous damping ratio and the RMS displacement ratios are provided. The charts cover a wide range of mass ratios and a practical design range for normalised RMS relative displacement. The use of design charts was demonstrated by a design example.

Acknowledgements

The Natural Sciences and Engineering Research Council of Canada and Rowan, Williams, Davis and Irwin Inc. have supported the initial stage of this work through the Industrial Postgraduate Scholarships program. The Ontario Ministry of Education continued the support through the Ontario Graduate Scholarships program.

Appendix A

See Tables A.1(a) and A.1(b).

Appendix B. Notation

List of symbols

D	side dimension of structure of square cross section
f_o	expected response frequency
f_r	frequency ratio
g	forcing ratio
H_x	complex frequency response function for primary system displacement
H_θ	complex frequency response function for auxiliary system rotation
h	distance between spring/damper (or wire rope spring) attachment point and pivot point
I_a	auxiliary system mass moment of inertia about the pivot point
i	$\sqrt{-1}$
K	particular vibration mode generalized stiffness
$k^{\min}$	minimum effective stiffness of wire rope spring
k_p^θ	pendulum rotational stiffness
M	particular vibration mode generalized mass
m_a	auxiliary mass
P_{CF}	peak correction factor
PF	peak factor
PF_r	peak factor of relative displacement
PF_x	peak factor of primary system displacement
PF_r^*	corrected peak factor of relative displacement
p	Rayleigh probability density function
R	ratio of RMS relative displacement to primary structure RMS displacement
R_d	general dynamic response
r_a	ratio of mass moment of inertia about pivot to that about center of mass
S_{Rd}	spectrum of general dynamic response
S_x	spectrum of primary system displacement
$S_{\ddot{x}_g}$	spectrum of base acceleration
S_θ	spectrum of auxiliary system rotation
T	duration of time over which peak factor is considered
X_r	relative displacement amplitude
$X_r^{\min}$	relative/representative displacement amplitude corresponding to minimum wire rope spring stiffness
x	displacement
x_r	relative displacement between auxiliary and primary systems
x_{tip}	tip displacement
$\ddot{x}_g$	base acceleration excitation
z	distance between auxiliary mass center and pivot point
β	damping ratio (% of critical)
β_a	damping ratio of auxiliary system (% of critical)
β_{e}	equivalent damping ratio of structure equipped with a TMD

β_{struct} inherent structural damping ratio (% of critical)
μ mass ratio
θ rotation
ω circular frequency
ω_a natural circular frequency of auxiliary system
ω_n natural circular frequency of primary system

Operators

$\dot{\cdot}$ differential with respect to time
$\bar{\cdot}$ average of quantity
$\tilde{\cdot}$ root-mean-square (RMS) of quantity
$\hat{\cdot}$ peak of quantity

Superscripts

^{L} limiting displacement
$^{\text{opt}}$ parameters corresponding to maximum β_e

Abbreviations

PDF probability density function
RMS root-mean-square
SDOF single-degree of freedom
TDOF two-degree of freedom
TMD tuned mass damper

References

[1] Gerges RR. Tuned mass dampers incorporating wire rope springs. Ph.D. thesis, London (Ontario, Canada): The University of Western Ontario; 2003.
[2] Gerges RR, Vickery BJ. Parametric experimental study of wire rope spring tuned mass dampers. Journal of Wind Engineering and Industrial Aerodynamics 2003;91:1363–85.
[3] Crandall SH, Mark WD. Random vibration in mechanical systems. New York (London): Academic Press; 1963.
[4] Davenport AG. The application of statistical concepts to the wind loading of structures. Institute for Civil Engineers 1961;19:449–72.
[5] Davenport AG. Note on the distribution of the largest value of a random function with application to gust loading. Institute for Civil Engineers 1964;28:187–96.
[6] Vickery BJ, Davenport AG. An investigation of the behaviour in wind of the proposed centrepoint tower in Sydney, Australia, Engineering Science Research Report No. BLWT-1-70, The University of Western Ontario, Faculty of Engineering Science, London (Ontario, Canada): Boundary Layer Wind Tunnel Laboratory; 1970.
[7] Vickery BJ, Steckley A. Aerodynamic damping and vortex excitation on an oscillating prism in turbulent shear flow. Journal of Wind Engineering and Industrial Aerodynamics 1993;49:121–40.